AUTHOR QUERIES – TO BE ANSWERED BY THE CORRESPONDING AUTHOR

As the publishing schedule is strict, please note that this might be the only stage at which you are able to thoroughly review your paper.
Please pay special attention to author names, affiliations and contact details, and figures, tables and their captions.
No changes can be made after publication.

The following queries have arisen during the typesetting of your manuscript. Please answer these queries by marking the required corrections at the appropriate point in the text.

Q1	While the online version of figures 3,5–10,12,13 will be in colour, we have been instructed to print the figures in black and white. Please note that if you have explicitly referred to colour in the caption this may affect the legibility of the figures in print.
Q2	Please provide publisher location [city/state/country] details for reference [3].
SQ1	Your supplementary material will be published online alongside your article and on rs.figshare.com exactly as the file(s) are provided. Therefore, please could you either confirm that your supplementary material is correct, or – if you have any changes to make to these files – email these along with your proof corrections to the journal inbox. Your ESM files are listed here for your convenience: esm.pdf

PROCEEDINGS A

Research

Check for updates

Author for correspondence:
Andrea Nobili
e-mail: andrea.nobili@unimore.it

Flexural edge waves generated by steady-state propagation of a loaded rectilinear crack in an elastically supported thin plate

Andrea Nobili[1], Enrico Radi[2] and Luca Lanzoni[3]

[1]Dipartimento di Ingegneria Enzo Ferrari, Università degli Studi di Modena e Reggio Emilia, via Vivarelli 10, 41125 Modena, Italy
[2]Dipartimento di Scienze e Metodi dell'Ingegneria, Università degli Studi di Modena e Reggio Emilia, via Amendola 2, 42122 Reggio Emilia, Italy
[3]Dipartimento di Economia e Tecnologia, Università degli Studi della Repubblica di San Marino, Via Salita alla Rocca 44, 47890 San Marino, Republic of San Marino

AN, 0000-0002-9657-5903

The problem of a rectilinear crack propagating at constant speed in an elastically supported thin plate and acted upon by an equally moving load is considered. The full-field solution is obtained and the spotlight is set on flexural edge wave generation. Below the critical speed for the appearance of travelling waves, a threshold speed is met which marks the transformation of decaying edge waves into edge waves propagating along the crack and dying away from it. Yet, besides these, and for any propagation speed, a pair of localized edge waves, which rapidly decay behind the crack tip, is also shown to exist. These waves are characterized by a novel dispersion relation and fade off from the crack line in an oscillatory manner, whence they play an important role in the far field behaviour. Dynamic stress intensity factors are obtained and, for speed close to the critical speed, they show a resonant behaviour which expresses the most efficient way to channel external work into the crack. Indeed, this behaviour is justified through energy considerations regarding the work of the applied load and the energy release rate. Results might be useful in a wide array of applications, ranging from fracturing and machining to acoustic emission and defect detection.

1. Introduction

Crack propagation in elastically supported thin structures made of brittle or quasi-brittle material is a common feature of many natural phenomena, such as ice fracturing and calving, rock fault planes and layered material failure, road pavement deterioration, surface coating detachment, to name only a few. In all instances, cracking takes place at the expense of the stored elastic energy, which is rapidly converted into stress waves travelling in the material and providing the so-called acoustic emission (AE). AE can be measured in the far-field and it lends a convenient indirect means to access the internal change in the material status. Besides travelling waves, moving in the bulk of the material, edge waves are usually excited and occur in a localized region near the boundaries [1,2]. edge waves tend to appear at smaller speed than travelling waves, owing to their lower energy content, and consequently are detected first [3,4]. Furthermore, edge waves are closely related to edge buckling [5].

When an external load moves on a thin structure, its speed might easily approach some resonant speed and produce dramatic effects [6]. This outcome is further enhanced by the presence of cracks in the structure. An intriguing example of this is the discovery that a ground effect machine may be successfully employed as ice breaker when operated at the system's critical speed [7]. The analysis of the effect of loads moving on elastic structures has been a long-standing subject of investigation, in the light of its many practical implications. Historically, much of this analysis has been directed by the desire to safely design bridges, rail tracks and road pavements under the ever-increasing demand of high-speed high-capacity transportation [8,9]. Recently, renewed interest has been drawn to model and design floating ice sheets as supporting structures for oil rigs, pipes, roads, runways and platforms [7]. Climate change and extensive investigation of the interaction between ice-shelf cracking and impinging sea-waves, in a process somewhat similar to that leading to edge waves excited by deep water surface waves [10], are also motivating further research in the field [11–13].

Remarkably, despite the broad interest and the wide range of application, only a handful of contributions may be found in the literature concerning fracture dynamics in elastically supported thin plates. The static solution to this problem was first considered in [14] and it was later extended in [15,16] to a weakly non-local foundation. In the classic references [17–19], several static problems for finite cracks in unsupported plates or shells are considered. The mathematical problem is related to that appearing in the study of crack propagation in couple-stress materials [20,21], although different boundary conditions (BCs) apply. In all cases, the combined effect of a moving load acting on a moving crack has never been investigated.

In this paper, the steady-state propagation of a rectilinear crack in a thin plate resting on a Winkler foundation and subject to a moving harmonic load applied at the crack flanks is considered. The spotlight is set on flexural edge waves generation as a result of this combination. In particular, it is observed that, compared with the classic subject of edge wave propagation at the boundary of a semi-infinite plate [22,23], a new edge wave arises out of the fact that propagation is restricted to the crack flanks. Besides, thorough investigation of the stress intensity factors reveals that the loading frequency may be tuned so as to either promote or hinder crack propagation in practical applications (consider, for instance, ice breaking as opposed to road pavement preservation). Finally, this solution may be used as a building block to tackle, through superposition, the problem of a general distributed load in steady-state motion on a cracked plate, where the load application is no longer restricted to the crack flanks, although it still moves with the crack tip.

The paper is organized as follows: §2 formulates the problem, which is then recast in the frequency domain in §3. The full-field solution is given in §4 and §5 discusses stress intensity factors (SIFs). Energy considerations supporting the non-monotonic behaviour of the SIFs are given in §6 along with the energy release rate (ERR) at the crack tip. Flexural edge wave solutions are considered in §7 and conclusions are drawn in §8. Finally, the electronic supplementary material presents the derivation of a conservative line integral, which extends to elastically

supported thin plates the analogous result obtained in [24] for steady-state crack propagation in rate-dependent plastic solids.

2. Problem formulation

(a) Field equations

We consider a semi-infinite rectilinear crack propagating along its length in an infinite Kirchhoff–Love (K-L) thin elastic plate (figure 1). The plate, of thickness h, is elastically supported by a Winkler foundation with stiffness k. A moving Cartesian reference frame, $(\hat{\xi}_1, \hat{\xi}_2, \hat{\xi}_3)$, is attached to the crack tip such that the linear crack corresponds to the negative part of the $\hat{\xi}_1$-axis, while the $\hat{\xi}_2$-axis measures the distance from the crack line of a point on the plate. The crack is propagating at constant speed c (steady-state propagation) with respect to a fixed reference frame (x_1, x_2, x_3). In this fixed frame, the governing equation for the transverse displacement of the plate, w, reads [7, §4.3]

$$D\triangle\triangle w + kw = -\rho h \partial_{tt} w + q, \tag{2.1}$$

being $\triangle = \partial_{x_1 x_1} + \partial_{x_2 x_2}$ the Laplace operator in two dimensions, q the transverse distributed load per unit area, D the plate bending stiffness and ρ the mass density per unit volume. The double Laplace operator is usually named biharmonic operator and it is denoted by ∇^4.

As is customary in a steady-state analysis, we set ourselves in the constant speed moving frame $(\hat{\xi}_1, \hat{\xi}_2, \hat{\xi}_3)$, with $\hat{\xi}_1 = x_1 - ct$, and assume $w = w(\hat{\xi}_1, \hat{\xi}_2)$, which bears no explicit time dependence. Then, equation (2.1) may be rewritten as

$$\hat{\nabla}^4 w + \kappa^{-2}\partial_{\hat{\xi}_1\hat{\xi}_1} w + \lambda^{-4} w = \frac{q}{D}, \tag{2.2}$$

having let the *characteristic lengths*

$$\lambda = \sqrt[4]{\frac{D}{k}} \quad \text{and} \quad \kappa = c^{-1}\sqrt{\frac{D}{\rho h}}, $$

together with the positive dimensionless ratio

$$\eta = \frac{\lambda}{\kappa} = c\frac{\sqrt{\rho h}}{\sqrt[4]{kD}}. $$

It is worth observing that equation (2.2) corresponds to the governing equation for a supported thin elastic plate subject to an axial compression of magnitude $D\kappa^{-2}$ [5] or for an unsupported cylindrical shell [14,25]. We introduce the dimensionless coordinates $(\xi_1, \xi_2) = \lambda^{-1}(\hat{\xi}_1, \hat{\xi}_2)$ and take $q \equiv 0$, with no loss of generality. Then, equation (2.2) becomes

$$\nabla^4 w + \eta^2 \partial_{\xi_1\xi_1} w + w = 0, \tag{2.3}$$

where $\nabla^4 = (\partial_{\xi_1\xi_1} + \partial_{\xi_2\xi_2})^2$ is the biharmonic operator in dimensionless coordinates. The special case $\eta = 0$ corresponds to the static problem, whose solution is given in [14]. Furthermore, we recall that, in a supported thin elastic plate, travelling wave solutions are admitted beyond a critical speed [7, §4.2]

$$c_{\mathrm{cr}} = \sqrt{2}\frac{\sqrt[4]{kD}}{\sqrt{\rho h}} \quad \Leftrightarrow \quad \eta = \eta_{\mathrm{cr}} = \sqrt{2}, \tag{2.4}$$

corresponding to the group speed and occurring at the dimensionless wavenumber

$$\mu = \mu_{\mathrm{cr}} = 1. $$

4

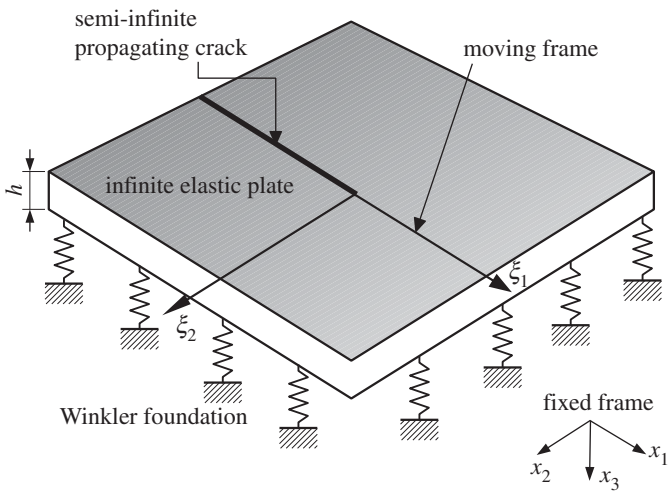rspa.royalsocietypublishing.org *Proc. R. Soc. A* 2017 0265

Figure 1. Rectilinear crack propagating at constant speed c in an elastic thin plate resting on a Winkler elastic foundation.

(b) Boundary conditions

Within the K-L theory, the bending moment, twisting moment and the equivalent shearing force are given by, respectively, [3]

$$m_{22} = -(\partial_{\xi_2 \xi_2} + \nu \partial_{\xi_1 \xi_1})w, \tag{2.5a}$$

$$m_{12} = \nu_0 \partial_{\xi_1 \xi_2} w, \tag{2.5b}$$

and
$$v_2 = -\lambda^{-1} \partial_{\xi_2}[\partial_{\xi_2 \xi_2} + (2 - \nu)\partial_{\xi_1 \xi_1}]w, \tag{2.5c}$$

all of them having being deprived of the common factor $D\lambda^{-2}$ and having let the shorthand notation $\nu_0 = 1 - \nu$. Besides, we let the slope

$$\phi = -\lambda^{-1}\partial_{\xi_2}w.$$

The BCs across the crack line $\xi_2 = 0$ and ahead of the crack tip, i.e. for $\xi_1 > 0$, are

— of kinematic nature, expressing continuity of displacement and slope,

$$[\![w_0(\xi_1)]\!] = [\![\phi_0(\xi_1)]\!] = 0, \quad \xi_1 > 0, \tag{2.6}$$

— of static nature, demanding continuity for the bending moment and the equivalent shearing force,

$$[\![m_0(\xi_1)]\!] = [\![v_0(\xi_1)]\!] = 0, \quad \xi_1 > 0, \tag{2.7}$$

where m_0 and v_0 are shorthands for m_{220} and v_{20}, respectively.

Here, $[\![f(0)]\!]$ denotes the jump of the function $f(\xi_2)$ across the crack line, namely $f(0^+) - f(0^-)$, while a zero subscript means evaluation at the crack line, i.e. $w_0(\xi_1) = w(\xi_1, 0)$.

As is well known, the solution of any linear fracture mechanics problem under general loading conditions may be obtained from the superposition of two simpler set-ups: the first set-up is obtained disregarding the crack and considering the given loading condition, the second set-up takes into account the presence of the crack, which is loaded by the force distribution found at the previous set-up. The latter problem may be further decomposed through harmonic expansion of the crack loading. In this paper, we are interested in investigating the effect of the crack and, consequently, only the second set-up will be considered. Indeed, it is assumed that the crack flanks

are loaded in a continuous fashion by a general harmonic term. Then, the BCs at the crack line $\xi_2 = 0$ are of static nature, namely

$$m_{22}(\xi_1, 0^\pm) = M_0 \exp(\iota a \xi_1) \quad \text{and} \quad v_2(\xi_1, 0^\pm) = \lambda^{-1} V_0 \exp(\iota a \xi_1), \quad \xi_1 < 0, \tag{2.8}$$

where $M_0 = M_0(a)$, $V_0 = V_0(a)$ are complex-valued and the dimensionless forcing frequency (in space) satisfies

$$\Im(a) < 0 \tag{2.9}$$

to ensure decay as $\xi_1 \to -\infty$. Hereinafter, ι is the imaginary unit, $\Re(s)$ and $\Im(s)$ denote the real and the imaginary part of $s \in \mathbb{C}$, respectively, and a superscript asterisk denotes complex conjugation, i.e. $s^* = \Re(s) - \iota \Im(s)$. We observe that equations (2.8), just like (2.6) and (2.7), entail four conditions in total, for they apply at both flanks of the crack (denoted by $\xi_2 = 0^\pm$). As a consequence of loading continuity, equations (2.7) hold on the entire crack line.

3. Analysis in the frequency domain

Let us define the bilateral (or full) Fourier transform of $w(\xi_1, \xi_2)$ along ξ_1 in the usual way [26]

$$\bar{w}(s, \xi_2) = \int_{-\infty}^{+\infty} w(\xi_1, \xi_2) \exp(\iota s \xi_1) \, d\xi_1.$$

In a similar fashion, the unilateral (or generalized, or half-range) transforms are introduced. The plus transform is defined as

$$\bar{w}^+(s, \xi_2) = \int_0^{+\infty} w(\xi_1, \xi_2) \exp(\iota s \xi_1) \, d\xi_1$$

and it is analytic in the complex half-plane $\Im(s) > \alpha_1$, provided that $\alpha_1 \in \mathbb{R}$ exists such that $w(\xi_1, \xi_2) \exp(-\alpha_1 \xi_1)$ is absolutely integrable with respect to ξ_1 in the interval $(0, +\infty)$. Likewise, the minus transform of w

$$\bar{w}^-(s, \xi_2) = \int_{-\infty}^0 w(\xi_1, \xi_2) \exp(\iota s \xi_1) \, d\xi_1$$

is analytic in the complex half-plane $\Im(s) < \alpha_2$ provided that α_2 can be found such that $w(\xi_1, \xi_2) \exp(\alpha_2 \xi_1)$ is absolutely integrable with respect to ξ_1 in the interval $(-\infty, 0)$. Consequently, assuming $\alpha_1 < 0 < \alpha_2$, the bilateral Fourier integral is related to the unilateral transforms through the connection

$$\bar{w}(s, \xi_2) = \bar{w}^+(s, \xi_2) + \bar{w}^-(s, \xi_2), \tag{3.1}$$

valid in the strip of analyticity $\mathcal{S} = \{s \in \mathbb{C} : \alpha_1 < \Im(s) < \alpha_2\}$ containing the real axis. In this strip, the inverse of the bilateral Fourier transform may be defined as:

$$w(\xi_1, \xi_2) = \frac{1}{2\pi} \int_{-\infty}^{+\infty} \bar{w}(s, \xi_2) \exp(-\iota s \xi_1) \, ds \tag{3.2}$$

and similarly for the inverse of the half-transforms.

Taking the Fourier transform of equation (2.3) in the ξ_1 variable, a linear constant coefficient ODE is obtained whose general solution is

$$\bar{w}(s, y) = A_1 \exp\left(-\sqrt{\Lambda_1}|\xi_2|\right) + B_1 \exp\left(\sqrt{\Lambda_1}|\xi_2|\right) + A_2 \exp\left(-\sqrt{\Lambda_2}|\xi_2|\right) + B_2 \exp\left(\sqrt{\Lambda_2}|\xi_2|\right), \tag{3.3}$$

wherein

$$\Lambda_{1,2} = s^2 \mp R(s) \quad \text{and} \quad R(s) = \sqrt{\eta^2 s^2 - 1}. \tag{3.4}$$

We observe that the factorization holds

$$\Lambda_1 \Lambda_2 = s^4 - \eta^2 s^2 + 1 = (s^2 - \beta^2)(s^2 - \beta^{*2}), \quad \beta = \sqrt{\frac{\eta^2}{2} + \iota \sqrt{1 - \frac{\eta^4}{4}}},$$

in which the roots $\pm\beta, \pm\beta^*$ are the branch points of the double square roots in (3.3). It is further observed that β is a complex number with unit modulus located in the first quadrant of the complex plane inasmuch as $0 \le \eta < \eta_{cr}$, while it sits on the real axis for $\eta \ge \eta_{cr}$. For a strip of analyticity about the real axis to be accessible and the inverse Fourier transform (3.2) meaningful, we need to have

$$\eta < \eta_{cr}. \tag{3.5}$$

This constraint amounts to requiring $c < c_{cr}$, where c_{cr} is the critical speed (2.4).

Let $w(\xi_1, \xi_2^+)$ and $w(\xi_1, \xi_2^-)$ be the restrictions of the displacement $w(\xi_1, \xi_2)$ in the upper and in the lower half of the (ξ_1, ξ_2)-plane, respectively, where it is understood that $\xi_2^+ \in (0, +\infty)$ and $\xi_2^- \in (-\infty, 0)$. The general solution of the ODE (2.3), bounded at infinity, retains only the A-terms,

$$\bar{w}(s, \xi_2^\pm) = A_1^\pm \exp\left(-\sqrt{\Lambda_1}|\xi_2^\pm|\right) + A_2^\pm \exp\left(-\sqrt{\Lambda_2}|\xi_2^\pm|\right), \tag{3.6}$$

where $A_1^\pm$ and $A_2^\pm$ are four *complex-valued* functions of s to be determined. The square root in (3.6) is made defined by choosing the Riemann sheet such that $\Re\left(\sqrt{\Lambda_{1,2}}\right) > 0$. To this aim, we locate the cuts according to the requirements

$$\Re(\Lambda_1) < 0 \quad \text{and} \quad \Im(\Lambda_1) = 0, \tag{3.7}$$

where the equality sets the cuts position, while the inequality warrants the proper orientation, see [3, §6.2.2] for more details. It is observed that adopting Λ_2 in (3.7) would lead to the same cut location in the light of the two-valued nature of the square root $R(s)$. Interestingly, the cut location is independent of v. We assume that $A_1^\pm$ and $A_2^\pm$ split into a symmetric and skew-symmetric part [15]:

$$A_i^\pm = \tfrac{1}{2}(\bar{A}_i \pm \Delta A_i), \quad i = 1, 2, \tag{3.8}$$

whence we have, for the restriction of (3.6) onto the ξ_1-axis,

$$\bar{w}_{0\pm}(s) = A_1^\pm + A_2^\pm. \tag{3.9}$$

Equation (2.6) may be written in terms of plus Fourier transforms

$$[\![\bar{w}_0^+]\!] = [\![\bar{\phi}_0^+]\!] = 0,$$

whence, using the general solution (3.6) and in view of equations (3.1), (3.8), (3.9), it is

$$\Delta A_1 + \Delta A_2 = [\![\bar{w}_0^-]\!] \tag{3.10a}$$

and

$$\sqrt{\Lambda_1}\bar{A}_1 + \sqrt{\Lambda_2}\bar{A}_2 = \lambda[\![\bar{\phi}_0^-]\!]. \tag{3.10b}$$

Likewise, the unilateral Fourier transform of equation (2.8) gives

$$\bar{m}_0^- = -\imath\frac{M_0}{s+a} \quad \text{and} \quad \bar{v}_0^- = -\imath\frac{\lambda^{-1}V_0}{s+a}, \tag{3.11}$$

valid in the semi-infinite region $\mathcal{S}_1 = \{s : \Im(s) < -\Im(a)\}$, which, by the inequality (2.9), contains the real axis. It is observed that M_0 and V_0 have dimension of length. Taking the full Fourier transform of the bending moment (2.5a) and of the shearing force (2.5c), we get

$$\bar{m} = -(\partial_{\xi_2\xi_2} - vs^2)\bar{w} \quad \text{and} \quad \bar{v} = -\lambda^{-1}\partial_{\xi_2}[\partial_{\xi_2\xi_2} - (2-v)s^2]\bar{w},$$

which, employing the solution (3.6) and using equations (3.1), (3.8), (3.11), gives

$$-[(\Lambda_1 - vs^2)A_1^\pm + (\Lambda_2 - vs^2)A_2^\pm] = \bar{m}_0^+ - \imath\frac{M_0}{s+a} \tag{3.12a}$$

and

$$\pm\lambda^{-1}\left\{\sqrt{\Lambda_1}[\Lambda_1 - (2-v)s^2]A_1^\pm + \sqrt{\Lambda_2}[\Lambda_2 - (2-v)s^2]A_2^\pm\right\} = \bar{v}_0^+ - \imath\frac{\lambda^{-1}V_0}{s+a} \tag{3.12b}$$

in the strip $S_0 = S \cap S_1$. Finally, Fourier transformation of equations (2.7), which really hold on the entire crack line, gives

$$(A_1 - vs^2)\Delta A_1 + (A_2 - vs^2)\Delta A_2 = 0 \tag{3.13a}$$

and

$$\sqrt{A_1}[A_1 - (2-v)s^2]\bar{A}_1 + \sqrt{A_2}[A_2 - (2-v)s^2]\bar{A}_2 = 0, \tag{3.13b}$$

according to which equations (3.12) reduce to

$$-\frac{1}{2}[(A_1 - vs^2)\bar{A}_1 + (A_2 - vs^2)\bar{A}_2] = \bar{m}_0^+ - \imath\frac{M_0}{s+a} \tag{3.14a}$$

and

$$\frac{1}{2}\left\{\sqrt{A_1}[A_1 - (2-v)s^2]\Delta A_1 + \sqrt{A_2}[A_2 - (2-v)s^2]\Delta A_2\right\} = \lambda\bar{v}_0^+ - \imath\frac{V_0}{s+a}. \tag{3.14b}$$

Conditions (3.13) are immediately fulfilled through letting

$$\Delta A_1 = -(A_2 - vs^2)\Delta A, \tag{3.15a}$$

$$\Delta A_2 = (A_1 - vs^2)\Delta A, \tag{3.15b}$$

$$\bar{A}_1 = -\sqrt{A_2}[A_2 - (2-v)s^2]\bar{A}, \tag{3.15c}$$

and

$$\bar{A}_2 = \sqrt{A_1}[A_1 - (2-v)s^2]\bar{A}, \tag{3.15d}$$

whence equations (3.10) become

$$(A_1 - A_2)\Delta A = [\![\bar{w}_0^-]\!], \tag{3.16a}$$

and

$$\sqrt{A_1 A_2}(A_1 - A_2)\bar{A} = \lambda[\![\bar{\phi}_0^-]\!]. \tag{3.16b}$$

Similarly, equations (3.14) give

$$(A_2 - A_1)K(s)\bar{A} = \bar{m}_0^+ - \imath\frac{M_0}{s+a}, \tag{3.17a}$$

and

$$(A_2 - A_1)K(s)\Delta A = \lambda\bar{v}_0^+ - \imath\frac{V_0}{s+a}, \tag{3.17b}$$

where the *kernel function* $K(s)$ is let as follows:

$$2(A_2 - A_1)K(s) = -\sqrt{A_1}[A_1 - (2-v)s^2](A_2 - vs^2) + \sqrt{A_2}[A_2 - (2-v)s^2](A_1 - vs^2). \tag{3.18}$$

In particular, in the limit as $\eta \to 0$, the function $4\imath K(s)$ in equation (3.18) reduces to the kernel (24) of [14]. Solving the system (3.16), which is linear in the unknown functions $\bar{A}, \Delta A$ and plugging the result in equations (3.17) provides the following pair of uncoupled inhomogeneous Wiener–Hopf (W-H) equations

$$K(s)[\![\bar{w}_0^-]\!] + \lambda\bar{v}_0^+ = \imath\frac{V_0}{s+a}, \tag{3.19a}$$

and

$$(A_1 A_2)^{-1/2}K(s)\lambda[\![\bar{\phi}_0^-]\!] + \bar{m}_0^+ = \imath\frac{M_0}{s+a}. \tag{3.19b}$$

4. Full-field solution

The kernel $K(s)$ is an even function of s and it possesses six roots all of which are, in the general case, of order unity (figure 2)

$$K(s) = 0 \quad \Leftrightarrow \quad s = \pm s_1, \quad \pm s_1^*, \quad \pm\imath r_1. \tag{4.1}$$
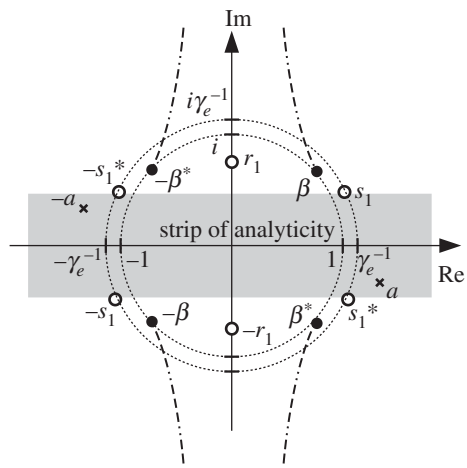
Figure 2. Branch cuts (dashed-dotted curves), branch points (solid dots) and zeros (circles) in the complex plane for the kernel function $K(s)$ in the regime $\eta < \eta_e$. Branch points and zeros are located on a circle (dotted) of radius 1 and γ_e^{-1}, respectively. The strip of analyticity $\mathcal{S}$ is also shown, together with the loading frequency a (cross).

Here, s_1 is taken to sit in the first quadrant of the complex plane,

$$s_1 = \gamma_e^{-1} \sqrt{\left(\frac{\eta}{\eta_e}\right)^2 + \imath \sqrt{1 - \left(\frac{\eta}{\eta_e}\right)^4}}, \quad \eta_e = \sqrt{2}\gamma_e,$$

having let $\gamma_e = \sqrt[4]{(1-\nu)\left(3\nu - 1 + 2\sqrt{2\nu^2 - 2\nu + 1}\right)}$, which is a well-known bending edge wave constant [22,23]. We observe that $\gamma_e \in \left[\sqrt{2}(\sqrt{5}-2)^{1/4}, 1\right]$ and its maximum $\gamma_e = 1$ is attained at $\nu = 0$. It is easy to see that s_1 is complex-valued for $\eta < \eta_e$ and it sits in the first quadrant of the complex plane on the circle of radius γ_e^{-1}. It can be proved that $\Im(s_1) > \Im(\beta)$ for $\eta < 1$, almost irrespectively of ν. According to the conditions (3.7), the double roots in the kernel $K(s)$ bring in two non-straight branch cuts which extend from $s = \beta, \beta^*$ to $-\beta, -\beta^*$ through $\imath\infty$, respectively. It is remarked that, for $\nu = 0$, it is $\gamma_e = 1$ and the roots $\pm s_1, \pm s_1^*$ coincide with the branch points for the double roots $\pm\beta, \pm\beta^*$, whence their order goes down to 1/2. Besides, in this case, $\eta_e = \eta_{\text{cr}}$.

In a similar fashion, we find the location of the purely imaginary roots $s = \pm\imath r_1$, being

$$r_1 = \gamma_m^{-1} \sqrt{\left(\frac{\eta}{\eta_m}\right)^2 + \sqrt{\left(\frac{\eta}{\eta_m}\right)^4 + 1}}, \quad \eta_m = \sqrt{2}\gamma_m$$

and we have defined the new constant

$$\gamma_m = \sqrt[4]{(1-\nu)\left(-3\nu + 1 + 2\sqrt{2\nu^2 - 2\nu + 1}\right)}.$$

We note that $\gamma_m \in \left[\left(2\sqrt{2}-1\right)^{1/4}/\sqrt{2}, \sqrt{2}\left(\sqrt{5}+2\right)^{1/4}\right]$ is a monotonic decreasing function of ν (figure 3). Conversely, r_1 is a real-valued monotonic increasing function of η, whose minimum $r_1 = \gamma_m^{-1}$ is attained in the static case $\eta = 0$, i.e. unlike s_1, this root never reaches the real axis. Indeed, in the special case $\eta = 0$ (stationary crack), we have

$$r_1 = \gamma_m^{-1} \quad \text{and} \quad s_1 = \gamma_e^{-1} \frac{\sqrt{2}}{2}(1 + \imath).$$
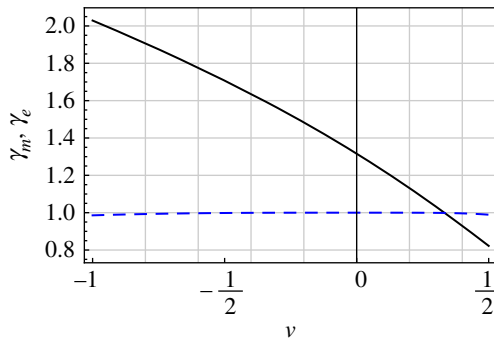
Figure 3. γ_m (solid, black) and γ_e (dashed, blue) as a function of Poisson ratio ν. (Online version in colour.)
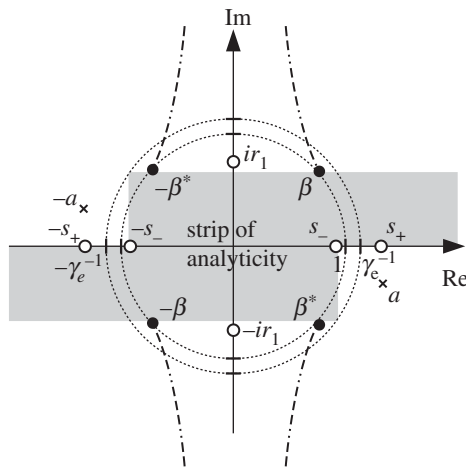
Figure 4. Branch cuts (dash-dot curves), branch points (solid dots) and zeros (circles) in the complex plane for the kernel function $K(s)$ in the regime $\eta_e \leq \eta < \eta_{cr}$. The strip of analyticity $\mathcal{S}$ is also shown as well as the loading frequency a (cross).

This situation is considered in [14], where the roots $\pm \imath r_1$ seem to have gone amiss. By contrast, for $\eta_e \leq \eta < \eta_{cr}$, s_1 turns real-valued and the root landscape (4.1) switches to (figure 4)

$$\pm s_-, \quad \pm s_+, \quad \pm \imath r_1,$$

where now $0 < s_- < \gamma_e^{-1} < s_+$ and

$$s_{\mp} = \gamma_e^{-1} \sqrt{\left(\frac{\eta}{\eta_e}\right)^2 \mp \sqrt{\left(\frac{\eta}{\eta_e}\right)^4 - 1}}.$$

In this case, the strip of analyticity $\mathcal{S}$ is taken to warrant the radiation (or Sommerfeld) condition of energy flowing from the load application zone to $\xi_1 \to -\infty$.

Let us define, for $d = v_0(3 + \nu)/4$ and for any chosen value $b > \alpha_{1,2} = \min\{\Im(s_1), \Im(\beta), r_1\}$,

$$F(s) = \frac{\sqrt{s^2 + b^2}\sqrt{s^2 - \beta^2}\sqrt{s^2 - \beta^{*2}}}{d(s^2 - s_1^2)(s^2 - s_1^{*2})(s^2 + r_1^2)} K(s). \tag{4.2}$$

The function $F(s)$ is even, deprived of zeros in a semi-infinite strip of analyticity $\mathcal{S}$, and it is such that $\lim_{|s| \to \infty} F(s) = 1$ in this strip. For such $F(s)$, the W-H logarithmic factorization [26, §3.2]

is applicable and it gives a plus and a minus function, respectively, denoted by $F^+(s)$ and $F^-(s)$, with the properties (see [27] for more details)

$$F(s) = F^+(s)F^-(s) \quad \text{and} \quad F^-(s) = F^+(-s).$$

Accordingly, system (3.19) reads

$$K^-(s)[\![\bar{w}_0^-]\!] + \frac{\lambda \bar{v}_0^+}{K^+(s)} = \imath V_0 \frac{1}{(s+a)K^+(s)}, \tag{4.3a}$$

and

$$\frac{K^-(s)}{\sqrt{s-\beta}\sqrt{s+\beta^*}} \lambda[\![\bar{\phi}_0^-]\!] + \frac{\sqrt{s+\beta}\sqrt{s-\beta^*}}{K^+(s)} \bar{m}_0^+ = \imath M_0 \frac{\sqrt{s+\beta}\sqrt{s-\beta^*}}{(s+a)K^+(s)}, \tag{4.3b}$$

where

$$K^\pm(s) = \sqrt{d} \frac{(s\pm s_1)(s\mp s_1^*)(s\pm \imath r_1)}{\sqrt{s\pm \imath b}\sqrt{s\pm \beta}\sqrt{s\mp \beta^*}} F^\pm(s)\sqrt{\pm \imath},$$

with the properties $K(s) = K^+(s)K^-(s)$ and $K^-(s) = K^+(-s)$. Here, it is understood that $\sqrt{\pm \imath} = \exp(\pm \imath \pi/4)$. For large values of $|s|$, we observe the asymptotic behaviour $K^\pm(s) \sim s^{3/2}$. Finally, the r.h.s. in equation (4.3) are split in terms of the sum of a plus and a minus function

$$\frac{\lambda \bar{v}_0^+}{K^+(s)} - \imath \frac{V_0}{s+a} \left(\frac{1}{K^+(s)} - \frac{1}{K^-(a)} \right) = \imath \frac{V_0}{(s+a)K^-(a)} - K^-(s)[\![\bar{w}_0^-]\!], \tag{4.4a}$$

and

$$\frac{\sqrt{s+\beta}\sqrt{s-\beta^*}}{K^+(s)} \bar{m}_0^+ - \imath \frac{M_0}{s+a} \left(\frac{\sqrt{s+\beta}\sqrt{s-\beta^*}}{K^+(s)} - \frac{\sqrt{a-\beta}\sqrt{a+\beta^*}}{K^-(a)} \right)$$

$$= \imath \frac{M_0}{s+a} \frac{\sqrt{a-\beta}\sqrt{a+\beta^*}}{K^-(a)} - \frac{K^-(s)}{\sqrt{s-\beta}\sqrt{s+\beta^*}} \lambda[\![\bar{\phi}_0^-]\!]. \tag{4.4b}$$

As, in system (4.4), the left (right) hand is represented by a function which is analytic in the upper (lower) complex half-plane with a common strip of regularity $\mathcal{S}_0$, it can be analytically continued into the whole complex plane. Indeed, continuation brings in two entire functions, $E_1(s)$ and $E_2(s)$, which are holomorphic over the whole complex plane. Appealing to Liouville's theorem, it is $E_1(s) \equiv E_2(s) \equiv 0$, in the light of the fact that the behaviour for large $|s|$ of either hands in equation (4.4) decays at least as fast as s^{-1}. Thus,

$$[\![\bar{w}_0^-]\!] = \imath \frac{V_0}{K^-(a)} \frac{1}{(s+a)K^-(s)} \tag{4.5}$$

and

$$\lambda[\![\bar{\phi}_0^-]\!] = \imath M_0 \frac{\sqrt{a-\beta}\sqrt{a+\beta^*}}{K^-(a)} \frac{\sqrt{s-\beta}\sqrt{s+\beta^*}}{(s+a)K^-(s)}. \tag{4.6}$$

Expressions for the unilateral Fourier transform of the bending moment and of the shearing force on the crack line follow immediately:

$$\bar{m}_0^+ = \imath \frac{M_0}{s+a} \left(1 - \frac{\sqrt{a-\beta}\sqrt{a+\beta^*}}{\sqrt{s+\beta}\sqrt{s-\beta^*}} \frac{K^+(s)}{K^-(a)} \right) \tag{4.7a}$$

and

$$\lambda \bar{v}_0^+ = \imath \frac{V_0}{s+a} \left(1 - \frac{K^+(s)}{K^-(a)} \right). \tag{4.7b}$$

It is observed that, according to Jordan's lemma [26], equations (4.5) and (4.6) satisfy both BCs (2.6) and, by the same argument, equations (4.7a) and (4.7b) imply the conditions (2.7).

Equations (3.6), (3.8), (3.15), (3.16) allow writing the full Fourier transform of the plate deflection

$$\bar{w}(s, \xi_2^\pm) = \frac{1}{2} \left(-\frac{\Lambda_2 - (2-\nu)s^2}{\sqrt{\Lambda_1}(\Lambda_1 - \Lambda_2)} \lambda[\![\bar{\phi}_0^-]\!] \mp \frac{\Lambda_2 - \nu s^2}{\Lambda_1 - \Lambda_2} [\![\bar{w}_0^-]\!] \right) e_1(s, \xi_2^\pm)$$

$$- \frac{1}{2} \left(-\frac{\Lambda_1 - (2-\nu)s^2}{\sqrt{\Lambda_2}(\Lambda_1 - \Lambda_2)} \lambda[\![\bar{\phi}_0^-]\!] \mp \frac{\Lambda_1 - \nu s^2}{\Lambda_1 - \Lambda_2} [\![\bar{w}_0^-]\!] \right) e_2(s, \xi_2^\pm),$$

having let the shorthand notation $e_{1,2}(s,\xi_2) = \exp\left(-\sqrt{\Lambda_{1,2}}|\xi_2|\right)$. In particular, on the crack line, it is $e_{1,2}(s,0) = 1$, whence

$$\bar{w}_{0\pm}(s) = -\left(\frac{v_0 s^2 - R(s)}{\sqrt{s^2 - R(s)}} - \frac{v_0 s^2 + R(s)}{\sqrt{s^2 + R(s)}}\right)\frac{\lambda[\![\bar{\phi}_0^-]\!]}{4R(s)} \pm \frac{1}{2}[\![\bar{w}_0^-]\!].$$

5. Stress-intensity factors

Stress-intensity factors (SIFs) can be determined from the behaviour of the relevant Fourier transform for large $|s|$. Indeed, equation (4.7a) gives

$$\bar{m}_0^+ \sim -\iota M_0 \frac{\sqrt{a-\beta}\sqrt{a+\beta^*}}{K^-(a)}\sqrt{\iota d}\,s^{-1/2},$$

whence, making use of the connection between the asymptotic expansion of a function and the expansion of its Fourier half-transform [26, §2.14.B], we get

$$m_0 \sim -\iota M_0 \frac{\sqrt{a-\beta}\sqrt{a+\beta^*}}{\Gamma(1/2)K^-(a)}\frac{\sqrt{\iota d}}{\sqrt{\xi_1}}, \quad \text{as } \xi_1 \to 0^+.$$

By the definition of the stress intensity factor [17] and recalling that $\sigma_{22} = 6h^{-2}m_{22}$ times the omitted term $D\lambda^{-2}$, we find

$$\hat{k}_1 = \lim_{\xi_1 \to 0^+}\sqrt{2\xi_1}\sigma_{\xi_2} = -6\iota\frac{DM_0}{\lambda^2 h^2}\frac{\sqrt{a-\beta}\sqrt{a+\beta^*}}{K^-(a)}\sqrt{\frac{2\iota d}{\pi}}. \tag{5.1}$$

The modulus of the dimensionless stress intensity factor $k_1 = (\lambda h)^2\hat{k}_1/(M_0 D)$ is plotted in figure 5 at fixed $\nu = 0.25$ as a function of the loading frequency. As expected, $|k_1|$ asymptotes to zero as $a^{-1/2}$ yet, remarkably, its decay is monotonic only for small speed η. Indeed, for η close to the critical speed, it displays an absolute maximum for $\Re(a)$ near 1, which becomes greater as $\eta \to \eta_{cr}$. The same resonant behaviour appears in figure 6, which shows the dependence of $|k_1|$ from the crack speed η. The role of ν is illustrated in figure 7 according to which resonance is stronger near the ends of the admissible range $\nu \in [-1, \frac{1}{2}]$.

Along the same line, it is easy to observe that, for large $|s|$, equation (4.7b) gives

$$\lambda\bar{v}_0^+ \sim -\iota V_0 \frac{\sqrt{\iota d}}{K^-(a)}s^{1/2},$$

whence we get

$$\lambda v_0 \sim -\iota V_0 \frac{\sqrt{\iota d}}{\Gamma(-1/2)K^-(a)}\xi_1^{-3/2},$$

and, therefore, in the light of the connection $\sigma_{23} = \frac{3}{2}h^{-1}v_2$,

$$\hat{k}_3 = \lim_{\xi_1 \to 0^+}\xi_1^{3/2}\sigma_{23} = \frac{3}{4}\iota\frac{DV_0}{\lambda^3 h}\frac{\sqrt{\iota d}}{\sqrt{\pi}K^-(a)}. \tag{5.2}$$

As shown in figures 5 and 6, the behaviour of $k_3 = \lambda^3 h/DV_0$ is similar to that of k_1, although it asymptotes to zero faster, as $|a|^{-3/2}$. Figure 8 brings along the role of ν at $\eta = 1$ and $\eta = \eta_{cr}$. In general, compared with $|k_1|$, $|k_3|$ appears much smaller.

Determination of k_2 requires dealing with the asymptotics of a full Fourier transform. Indeed, Fourier transformation of the twisting moment (2.5b) gives

$$\bar{m}_{12} = \iota v_0 s \partial_{\xi_2}\bar{w} = \mp\iota v_0 s\left[\sqrt{\Lambda_1}A_1^\pm e_1(s,\xi_2) + \sqrt{\Lambda_2}A_2^\pm e_2(s,\xi_2)\right]$$

$$= \pm\iota\frac{v_0 s}{2(\Lambda_1 - \Lambda_2)}\{[(\Lambda_2 - (2-\nu)s^2)\lambda[\![\bar{\phi}_0^-]\!] \pm \sqrt{\Lambda_1}(\Lambda_2 - \nu s^2)[\![\bar{w}_0^-]\!]]e_1(s,\xi_2)$$

$$- [(\Lambda_1 - (2-\nu)s^2)\lambda[\![\bar{\phi}_0^-]\!] \pm \sqrt{\Lambda_2}(\Lambda_1 - \nu s^2)[\![\bar{w}_0^-]\!]]e_2(s,\xi_2)\},$$

12

rspa.royalsocietypublishing.org Proc. R. Soc. A 20170265
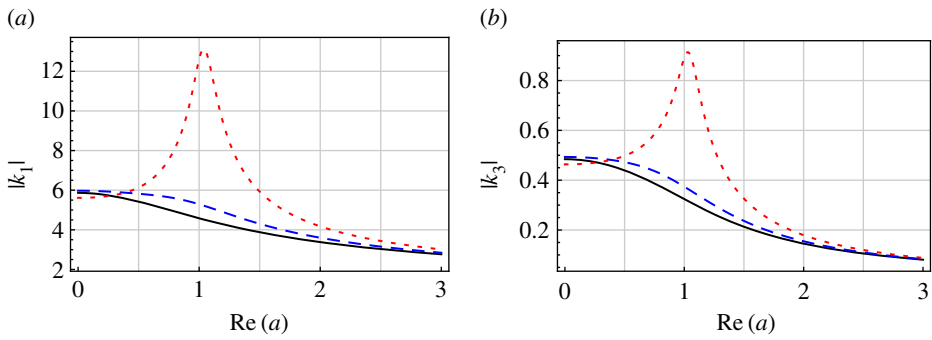...

Figure 5. Modulus of the dimensionless stress intensity factors $|k_1|$ (a) and $|k_3|$ (b) versus $\Re(a)$ for $\Im(a) = -0.1\imath$, $\nu = 0.25$ and $\eta = 0.5$ (solid, black), 1 (dashed, blue) and η_{cr} (dotted, red). (Online version in colour.)
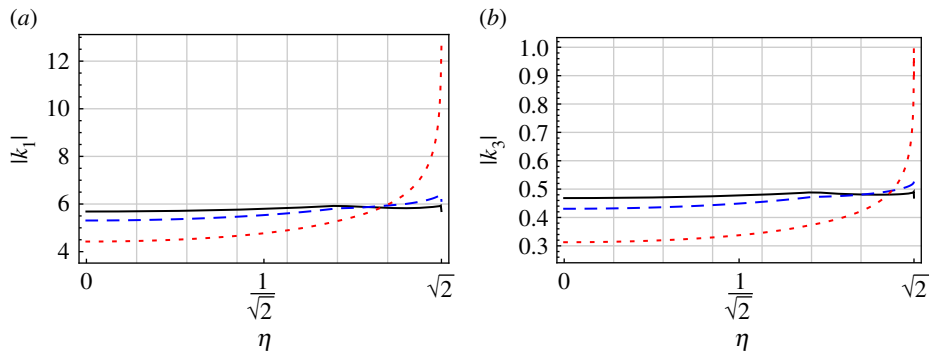

Figure 6. $|k_1|$ (a) and $|k_3|$ (b) versus speed η for $\Im(a) = -0.1\imath$, $\nu = 0.25$ and $\Re(a) = 0.25$ (solid, black), 0.5 (dashed, blue) and 1 (dotted, red). (Online version in colour.)
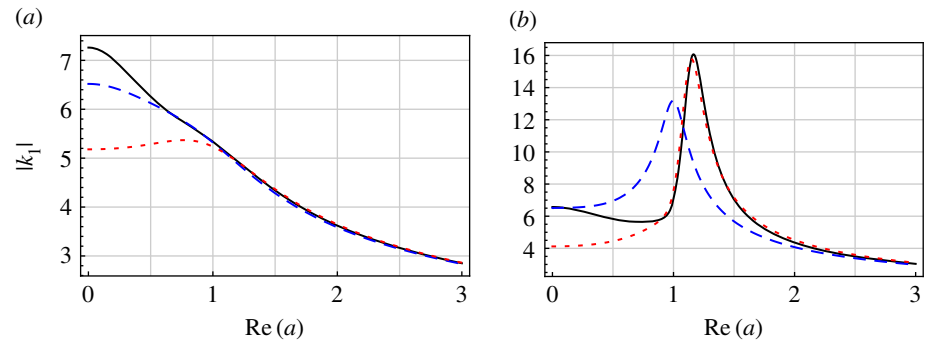

Figure 7. $|k_1|$ versus $\Re(a)$ for $\Im(a) = -0.1\imath$, $\nu = -1$ (solid, black), 0 (dashed, blue), 0.5 (dotted, red) and $\eta = 1$ (a), $\eta = \eta_{cr}$ (b). (Online version in colour.)

which, on the crack line, reduces to

$$
\bar{m}_{120} = \imath \frac{v_0}{2} s \left(\mp \lambda [\![\bar\phi_0^-]\!] - \frac{\sqrt{\varLambda_1}(\varLambda_2 - \nu s^2) - \sqrt{\varLambda_2}(\varLambda_1 - \nu s^2)}{\varLambda_2 - \varLambda_1} [\![\bar{w}_0^-]\!] \right).
$$

It is observed that the first term in parenthesis in this equation is a minus function, which brings no contribution for $\xi_1 > 0$. Conversely, the second term is analytic in a semi-infinite strip around the real axis and it is neither plus nor minus. Some straightforward asymptotic analysis
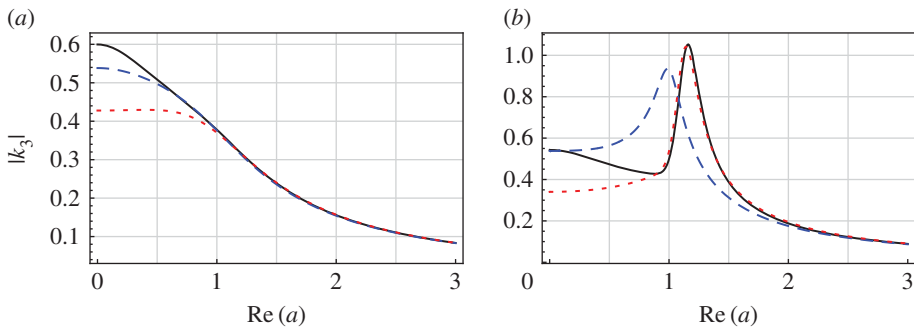
Figure 8. $|k_3|$ versus $\Re(a)$ for $\Im(a) = -0.1\iota$, $\nu = -1$ (solid, black), 0 (dashed, blue), 0.5 (dotted, red) and $\eta = 1$ (*a*), $\eta = \eta_{cr}$ (*b*). (Online version in colour.)

Q1

of equation (4.5) gives, for large $|s|$,

$$[\![\bar{w}_0^-]\!] \sim \iota V_0 \frac{1}{\sqrt{-\iota d}K^-(a)} s^{-5/2},$$

whence

$$\bar{m}_{120} \sim \frac{1}{4} V_0 \frac{1-\nu^2}{\sqrt{-\iota d}K^-(a)} s^{-1/2}, \quad \text{as } |s| \to +\infty.$$

As the asymptotics of the full Fourier transform is available, we employ Abel's theorem [28] to get

$$m_{120} = \frac{1}{4} V_0 \frac{\sqrt{2\pi}(1-\nu^2)}{\sqrt{-\iota d}K^-(a)} \xi_1^{-1/2}, \quad \text{as } \xi_1 \to 0^+,$$

whence

$$\hat{k}_2 = \lim_{\xi_1 \to 0^+} \sqrt{2\xi_1}\sigma_{12} = 3\frac{DV_0}{\lambda^2 h^2} \frac{\sqrt{\pi}(1-\nu^2)}{\sqrt{-\iota d}K^-(a)}, \tag{5.3}$$

which is proportional to k_3. It is remarked that SIFs have been determined within the framework of the K-L theory, which neglects shear deformation.

6. Stored energy and energy release rate

The resonant behaviour of the SIFs can be most easily explained evaluating the energy fed into the system by the applied load, which, according to Betti's theorem, is given by

$$W = \frac{1}{2}D\lambda^{-2}\int_{-\infty}^{0}(m_0[\![\phi_0]\!] + v_0[\![w_0]\!])\lambda \, d\xi_1$$

$$= \frac{1}{2}D\lambda^{-2}\int_{-\infty}^{0}(M_0\lambda[\![\phi_0]\!] + V_0[\![w_0]\!])\exp(\iota a\xi_1) \, d\xi_1$$

$$= \frac{1}{4}\iota D\lambda^{-2}(M_0^2 W_1 + V_0^2 W_2),$$

where

$$W_1 = \frac{(a-\beta)(a+\beta^*)}{aK^-(a)^2} \quad \text{and} \quad W_2 = \frac{1}{aK^-(a)^2}.$$

The dimensionless energies introduced by the bending moment and by the shearing force, respectively, W_1 and W_2, are plotted in figure 9 as a function of the applied load frequency a. It appears that a local maximum in the energy input occurs for $a \approx 1$, which is responsible for the non-monotonic behaviour of the SIFs. Similarly, figure 10 presents W_1 and W_2 as a function of the crack propagation speed η.
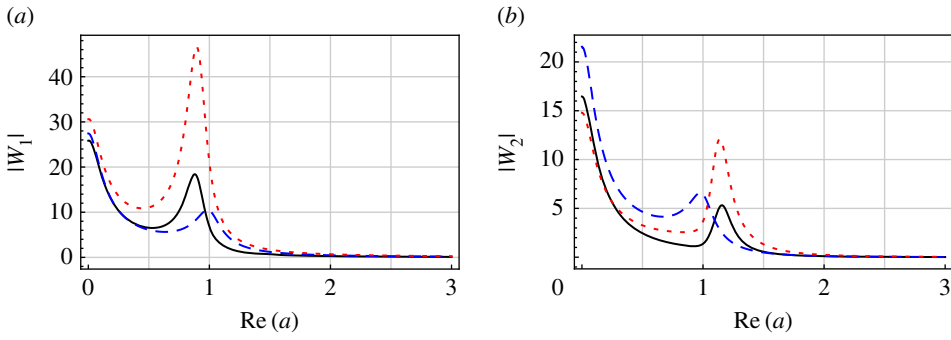
(a) (b)

Figure 9. Bending moment dimensionless energy input $|W_1|$ (a) and shearing force dimensionless energy input $|W_2|$ (b) versus $\Re(a)$ for $\Im(a) = -0.1\iota$, $\eta = \eta_\sigma$ and $\nu = -1$ (solid, black), 0 (dashed, blue) and 0.5 (dotted, red). (Online version in colour.)
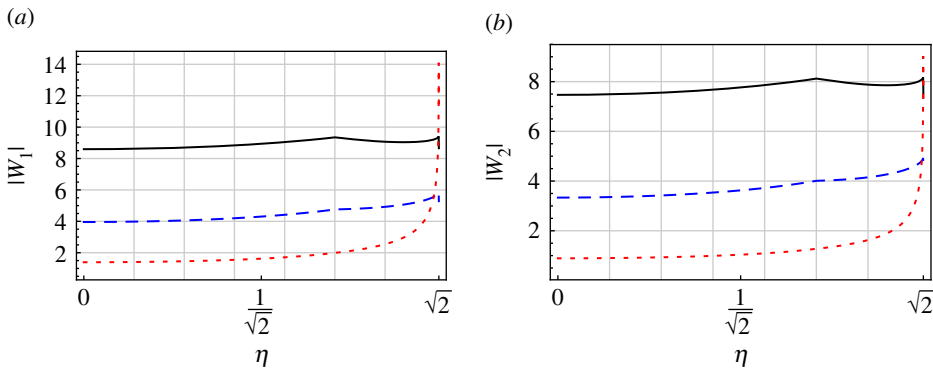
(a) (b)

Figure 10. Bending moment dimensionless energy input $|W_1|$ (a) and shearing force dimensionless energy input $|W_2|$ (b) versus η for $\Im(a) = -0.1\iota$, $\nu = 0.25$ and $\Re(a) = 0.25$ (solid, black), 0.5 (dashed, blue) and 1 (dotted, red). (Online version in colour.)

Q1

A more rigorous argument pertains to the ERR at the crack tip, G_{tip}, which may be determined through the conservative integral I. A derivation of this integral in the case of elastically supported thin plates is presented in the electronic supplementary material (see also [29]). To relate I to the near-tip fields, we consider a suitable contour Γ constituted by a vanishingly thin rectangular box, centred at the crack tip, with sides $2\delta_1 \ll 2\delta_2$ parallel to the ξ_1 and ξ_2 axes, respectively, by the crack flanks Γ^+ and Γ^- and finally closed by the far-field circle Γ_R, with radius R (figure 11). As we shrink the rectangular box down to the crack tip, i.e. $\delta_{1,2} \to 0^+$, and simultaneously let $R \to +\infty$, we get

$$I = \lim_{\delta_{1,2} \to 0^+} \int_{\Gamma^+} (m_{22}\partial_{\xi_1}[\![\phi_2]\!] + q_2\partial_{\xi_1}[\![w]\!] + m_{12}\partial_{\xi_1}[\![\phi_1]\!])\lambda \, d\xi_1 + G_{\text{tip}} = 0,$$

in the light of the fact that $\lim_{R \to +\infty} \int_{\Gamma_R} = 0$ and G_{tip} is the contribution of the small box centred at the crack tip. Taking the limit of the integral term and part integrating twice leads to

$$G_{\text{tip}} = -\int_{-\infty}^{0} (m_{22}\partial_{\xi_1}[\![\phi_2]\!] + v_2\partial_{\xi_1}[\![w]\!])\lambda \, d\xi_1$$

$$= -\frac{D}{\lambda^2} \int_{-\infty}^{0} \partial_{\xi_1}(M_0\lambda[\![\phi_0]\!] + V_0[\![w_0]\!]) \exp(\iota a\xi_1) \, d\xi_1$$

$$= \iota D\lambda^{-2} a \int_{-\infty}^{0} (M_0\lambda[\![\phi_0]\!] + V_0[\![w_0]\!]) \exp(\iota a\xi_1) \, d\xi_1 = 2\iota aW,$$

15

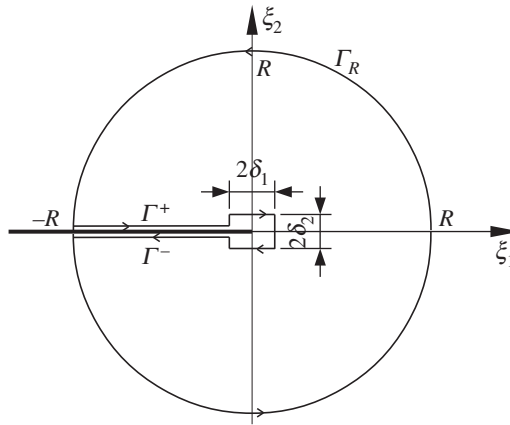rspa.royalsocietypublishing.org Proc. R. Soc. A 20170265

Figure 11. Integration path for evaluation of G_{tip}.

for boundary terms vanish and recalling the definition of the Kirchhoff equivalent shearing force $v_2 = q_2 + \partial_{\xi_1} m_{12}$. It is concluded that, for steady-state crack propagation, the ERR, which is readily seen to be proportional to the SIFs squared, may be related to the work of the applied loads. Therefore, the resonant behaviour displayed by the SIFs represents the most efficient way to channel energy from the applied load to the crack tip and thus promote fracturing.

7. Edge waves at the crack flanks

In this section, we provide some physical insight into the afore-obtained results. Looking for solutions of equation (2.3) in the form of a edge wave [23] for, say, the top half-plate,

$$w(\xi_1, \xi_2^+) = \exp[-\mu(\imath\xi_1 + \zeta\xi_2^+)] \tag{7.1}$$

and, plugging this expression in the governing equation (2.3), we obtain, for the attenuation index,

$$\zeta_{1,2} = \sqrt{1 \pm \frac{\sqrt{\eta^2\mu^2 - 1}}{\mu^2}}. $$

The sign for ζ is chosen so as to warrant decay as $\xi_2 \to +\infty$, i.e. it is such that $\Re(\mu\zeta) > 0$. Indeed, μ is generally a complex number such that

$$\Im(\mu) > 0. \tag{7.2}$$

Consideration of homogeneous BCs gives the dispersion relation

$$(1 - v^2)\mu^4 + \left(2v_0\sqrt{1 - \eta^2\mu^2 + \mu^4} - \eta^2\right)\mu^2 + 1 = 0, $$

which, upon rationalizing, gives the solution curve

$$\eta^2 = \gamma_e^4\mu^2 + \mu^{-2}. \tag{7.3}$$

This quadratic equation in μ^2 is plotted in figure 12 and it possesses two positive real roots provided that the moving frame speed η exceeds the threshold speed $\eta_e \leq \eta_{cr}$. This threshold corresponds to the minimum speed of the phase velocity (see [23]) and it occurs at the dimensionless wavenumber $\mu = \gamma_e^{-1} \geq 1$. For $\eta < \eta_e$, μ is complex-valued and we find a pair of decaying edge waves whose wavenumber corresponds to the single complex solution of (7.3)
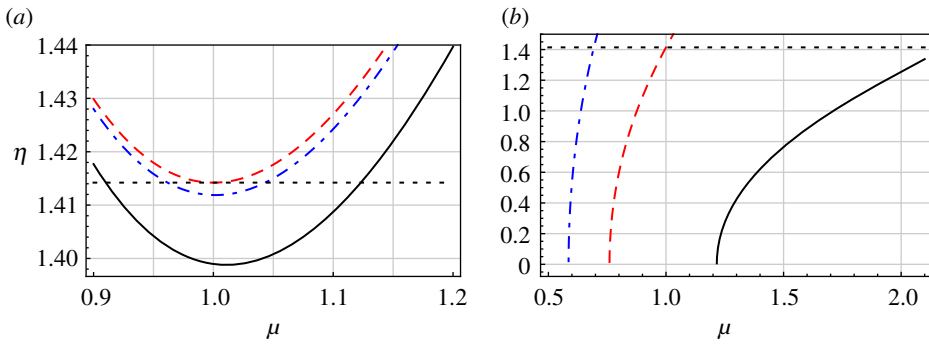
Figure 12. Edge wave dispersion curves (*a*) and decaying edge wave dispersion curves (*b*) for $\nu = 0.5$ (solid, black), $\nu = 0$ (dashed, red), $\nu = -0.5$ (dashed-dotted, blue). A minimum threshold speed $\eta_e = \sqrt{2}\gamma_e$ exists for propagating edge waves to appear (here plotted as a dotted curve only for $\nu = 0$). (Online version in colour.)

Q1

complying with (7.2) and whose attenuation indexes are given by the pair of positive real values

$$\zeta_{1,2} = \sqrt{1 \pm \gamma_e^2}, \tag{7.4}$$

irrespectively of the wavenumber. This solution exists only along the crack flanks, i.e. behind the propagating crack tip, and for it the sign of $\Re(\mu)$ is irrelevant.

For $\eta \geq \eta_e$, edge waves become propagating along the crack flanks with a pair of real wavenumbers s_-, s_+ and the same pair of attenuation indices (7.4), for a total of four edge wave solutions. These occur at smaller speed yet lower (higher) wavenumber s_- (respectively, s_+) than travelling wave solutions. In the special case $\nu = 0$, they occur simultaneously, for $\eta = \eta_e = \eta_{cr}$ and equation (7.3) admits the double root $\mu = 1$ (figure 12) and the attenuation index ζ is either $\sqrt{2}$ or zero, whence only one proper edge wave solution really exists, the other solution corresponding to a travelling wave.

In the frequency domain analysis, edge wave solutions are closely related to the complex root s_1, which expresses the wavenumber μ (as already remarked, for this class of solutions, the sign of $\Re(\mu)$ is immaterial, which amounts to considering either s_1 or $-s_1^*$). Indeed, this root is a pole for the minus transforms (4.5), (4.6) and, when considered in the inversion integral (3.2), it gives a solution of the form (7.1). Such solution represents decaying (along ξ_1) edge vibrations, which turn into proper edge waves, propagating at $\xi_1 \to -\infty$, provided that $\eta \geq \eta_e$. Indeed, beyond the minimum speed η_e, s_1 moves onto the real axis and it separates in the pair of poles s_+ and s_-. In this context, when $\nu = 0$, the roots s_1 and $-s_1^*$ become of fractional order and no longer correspond to exponential solutions.

Alongside the edge wave solution (7.1), we look for solutions in the form of exponentially decaying localized waves

$$w(\xi_1, \xi_2^+) = \exp[\mu(\xi_1 - \zeta \xi_2^+ t)], \quad \xi_1 \leq 0, \tag{7.5}$$

assuming $\mu > 0$ in consideration of the fact that the crack flank extends along the negative ξ_1-axis. Plugging this solution into the plate equation (2.3) gives, for the attenuation index, the complex-conjugated pair

$$\zeta_{1,2} = \sqrt{-1 \pm \imath \frac{\sqrt{\eta^2 \mu^2 + 1}}{\mu^2}},$$

where the square root is chosen as to have $\Re(\zeta_{1,2}) > 0$ and, accordingly, decay as $\xi_2 \to +\infty$. Consideration of load-free BCs yields a novel dispersion relation

$$(1 - \nu^2)\mu^4 + \left(\eta^2 - 2\nu_0\sqrt{\mu^4 + \eta^2\mu^2 + 1}\right)\mu^2 + 1 = 0,$$
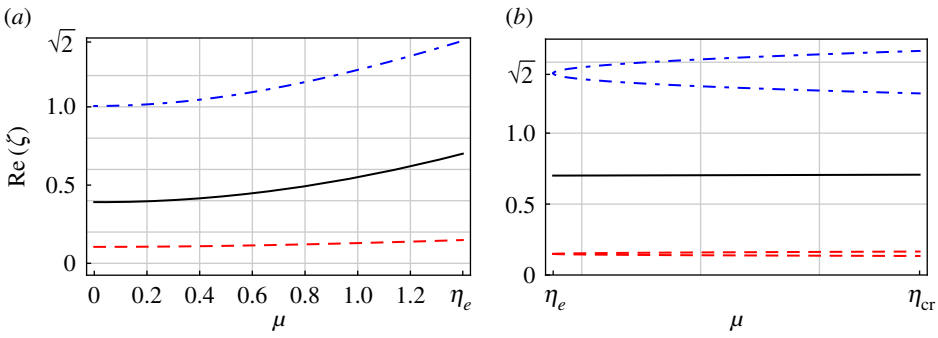
Figure 13. Attenuation rate $\Re(\mu\zeta)$ for edge wave solutions of the form (7.1) and $\zeta = \sqrt{1 \pm \gamma_2^2}$ (respectively, dashed-dotted, blue and dashed, red) compared with localized solutions (7.5) with $\zeta = \sqrt{-1 + \imath \gamma_m^2}$ (solid, black), at $\nu = 0.5$. In the speed range $\eta < \eta_e$ (a), only decaying edge waves are present, whereas in the range $\eta_e \leq \eta < \eta_{cr}$ (b), propagating edge waves appear and the corresponding curves bifurcate. (Online version in colour.) **Q1**

whose single positive solution is plotted in figure 12. This dispersion curve corresponds to the solution curve

$$\eta^2 = \gamma_m^4 \mu^2 - \mu^{-2}, \quad \mu > \gamma_m^{-1}.$$

which, just like (7.3), describes a parabola in μ^2. Clearly, for any given speed η, this equation defines two real wavenumbers, although only one of these complies with the inequality, namely

$$\mu = r_1 > \gamma_m^{-1}.$$

For this wavenumber, we see that the attenuation index ζ is given by the complex-conjugated pair

$$\zeta_{1,2} = \sqrt{-1 \pm \imath \gamma_m^2}. \tag{7.6}$$

This class of edge disturbances are related to the root $\imath r_1$ through Fourier inversion. Figure 13 compares the attenuation rates $\Re(\mu\zeta)$ of all solutions. It appears that, in the regime $\eta < \eta_e$, any far-field condition (i.e. at large ξ_2) is satisfied by a linear combination of one decaying wave with $\zeta = \sqrt{1 - \gamma_e^2}$ and one localized wave. Conversely, in the speed range $\eta_e \leq \eta < \eta_{cr}$, any far-field condition is realized by a linear combination of two propagating edge waves.

To recapitulate, three edge wave solutions exist, which correspond to the zeros of the kernel function (3.18) in the complex plane, namely

— s_1 (or $-s_1$) corresponds to the wavenumber of a pair of decaying (along the crack flank) edge waves with real attenuation indexes, provided that the crack moving speed η rests below the threshold speed η_e;
— conversely, for $\eta_e \leq \eta < \eta_{cr}$, s_1 separates into a pair of real numbers, $s_- \leq 1 \leq s_+$, that describe the wavenumbers of two pairs of propagating edge waves, with the same pair of real attenuation indexes occurring at the previous regime;
— for any speed, $\imath r_1$ corresponds to a pair of exponentially decaying solutions, localized at the back of the crack tip, associated with the positive wavenumber $r_1 > \gamma_m^{-1}$ and with a complex-conjugated pair of attenuation indexes.

8. Conclusion

In this paper, the full-field solution for the steady-state propagation of a rectilinear crack in an elastically supported thin plate is given through the W-H method. A harmonic moving load is applied at the moving crack flanks. Focus is set on the analysis of flexural edge waves propagating

as a result of the combined effect of crack extension and load motion. It is found that this combination brings in two regimes and three types of waves. Indeed, the solution identifies two threshold speeds, namely the critical speed η_{cr}, for travelling waves to appear in the bulk of the plate, and the edge wave speed $\eta_e \leq \eta_{cr}$, which corresponds to the speed of edge waves at the boundary of a semi-infinite thin plate. These two threshold speeds coincide when $\nu = 0$, for it is shown that edge waves collapse into travelling waves. When the propagation speed η is smaller than η_e, a pair of edge waves exist that decay in an oscillatory manner along the crack-flanks and rapidly fade off away from the crack line with real attenuation index. Rapid attenuation away from the crack line remains for $\eta \geq \eta_e$, yet edge waves become four and they propagate indefinitely along the crack flanks. For any propagation speed, a new type of edge wave is met which is highly localized behind the crack tip. Indeed, two such waves exist which decay with the real exponent along the crack, yet they are associated with a complex-conjugated pair of attenuation indexes, which amounts to oscillatory decay away from the crack line. For this localized edge wave, a novel dispersion relation is given and it is shown that its attenuation stands between the attenuation of decaying and propagating waves in the speed regime $\eta < \eta_e$. Consequently, this wave may be put to advantage for defect detection. This localized solution seems somewhat connected with the dynamic edge effect in cylindrical shells [30], for which curvature plays the role that is here taken by the elastic support.

Dynamic stress intensity factors are also obtained and they show a remarkable resonant behaviour, which is explained in the light of the ERR at the crack tip. Resonance may be successfully exploited in many practical applications, for instance to speed up ice breaking or sawing, or carefully avoided in many others, for example, to prevent rapid deterioration in pavements or layered materials. Finally, the work of the applied loading is shown to be proportional to the ERR at the crack tip through developing a conservative integral for elastically supported thin plates.

References

1. Norris A, Krylov V, Abrahams I. 2000 Flexural edge waves and comments on 'A new bending wave solution for the classical plate equation' [J. Acoust. Soc. Am. 104, 2220–2222 (1998)]. *J. Acoust. Soc. Am.* **107**, 1781–1784. (doi:10.1121/1.428457)
2. Kaplunov J, Nobili A. 2015 The edge waves on a Kirchhoff plate bilaterally supported by a two-parameter elastic foundation. *J. Vib. Control* **23**, 2014–2022. (doi:10.1177/1077546315606838)

Q2 3. Graff KF. 2012 *Wave motion in elastic solids*. Courier Corporation.
4. Lawrie JB, Kaplunov J. 2012 Edge waves and resonance on elastic structures: an overview. *Math. Mech. Solids* **17**, 4–16. (doi:10.1177/1081286511412281)
5. Destrade M, Fu Y, Nobili A. 2016 Edge wrinkling in elastically supported pre-stressed incompressible isotropic plates. *Proc. R. Soc. A.* **472**, 20160410. (doi:10.1098/rspa.2016.0410)
6. Frýba L. 2013 *Vibration of solids and structures under moving loads*, vol. 1. Berlin, Germany: Springer Science & Business Media.
7. Squire V, Hosking R, Kerr A, Langhorne P. 2012 *Moving loads on ice plates*, vol. 45. Berlin, Germany: Springer Science & Business Media.
8. Kim SM, Roesset J. 1998 Moving loads on a plate on elastic foundation. *J. Eng. Mech.* **124**, 1010–1017. (doi:10.1061/(ASCE)0733-9399(1998)124:9(1010))
9. Sun L. 2005 Dynamics of plate generated by moving harmonic loads. *J. Appl. Mech.* **72**, 772–777. (doi:10.1115/1.1993669)
10. Guza R, Davis R. 1974 Excitation of edge waves by waves incident on a beach. *J. Geophys. Res.* **79**, 1285–1291. (doi:10.1029/JC079i009p01285)

11. Wadhams P. 2000 *Ice in the ocean*. Boca Raton, FL: CRC Press.
12. Balmforth N, Craster R. 1999 Ocean waves and ice sheets. *J. Fluid Mech.* **395**, 89–124. (doi:10.1017/S0022112099005145)
13. Lu W, Lubbad R, Løset S. 2015 Out-of-plane failure of an ice floe: radial-crack-initiation-controlled fracture. *Cold. Reg. Sci. Technol.* **119**, 183–203. (doi:10.1016/j.coldregions.2015.08.009)
14. Ang DD, Folias ES, Williams ML. 1963 The bending stress in a cracked plate on an elastic foundation. *J. Appl. Mech.* **30**, 245–251. (doi:10.1115/1.3636519)
15. Nobili A, Radi E, Lanzoni L. 2014 A cracked infinite Kirchhoff plate supported by a two-parameter elastic foundation. *J. Eur. Ceram. Soc.* **34**, 2737–2744. (doi:10.1016/j.jeurceramsoc.2013.12.029)
16. Nobili A, Radi E, Lanzoni L. 2016 On the effect of the backup plate stiffness on the brittle failure of a ceramic armor. *Acta Mech.* **227**, 159–172. (doi:10.1007/s00707-015-1412-5)
17. Sih G. 1991 Strain energy density theory applied to plate-bending and shell problems. In *Mechanics of fracture initiation and propagation*, pp. 57–98. Berlin, Germany: Springer.
18. Tada H, Paris P, Irwin G. 2000 *Stress analysis of cracks handbook*, 3rd edn. New York, NY: ASME Press.
19. Sih G (ed.). 2013 *Plates and shells with cracks: a collection of stress intensity factor solutions for cracks in plates and shells*. 1977th edn. Mechanics of Fracture. Berlin, Germany: Springer.
20. Radi E. 2007 Effects of characteristic material lengths on mode III crack propagation in couple stress elastic–plastic materials. *Int. J. Plast.* **23**, 1439–1456. (doi:10.1016/j.ijplas.2007.01.002)
21. Morini L, Piccolroaz A, Mishuris G, Radi E. 2013 On fracture criteria for dynamic crack propagation in elastic materials with couple stresses. *Int. J. Eng. Sci.* **71**, 45–61. (doi:10.1016/j.ijengsci.2013.05.005)
22. Konenkov Y. 1960 A Rayleigh-type flexural wave. *Sov. Phys. Acoust.* **6**, 122–123.
23. Kaplunov J, Prikazchikov D, Rogerson G, Lashab M. 2014 The edge wave on an elastically supported Kirchhoff plate. *J. Acoust. Soc. Am.* **136**, 1487–1490. (doi:10.1121/1.4894795)
24. Freund L, Hutchinson J. 1985 High strain-rate crack growth in rate-dependent plastic solids. *J. Mech. Phys. Solids.* **33**, 169–191. (doi:10.1016/0022-5096(85)90029-8)
25. Sih G, Setzer D. 1964 Discussion: 'The bending stress in a cracked plate on an elastic foundatio (Ang, DD, Folias, ES, and Williams, ML, 1963, ASME J. Appl. Mech., 30, pp. 245–251)'. *J. Appl. Mech.* **31**, 365–366. (doi:10.1115/1.3629639)
26. Roos B. 1969 *Analytic functions and distributions in physics and engineering*. New York, NY: John Wiley & Sons.
27. Nobili A, Radi E, Lanzoni L. 2017 A Wiener-Hopf system of equations in the steady-state propagation of a rectilinear crack in an infinite elastic plate. In *Integral methods in science and engineering*, vol. 1, pp. 237–246. New York, NY: Birkhäuser.
28. Noble B. 1988 *Methods based on the Wiener-Hopf technique for the solution of partial differential equations*. New York, NY: Chelsea Pub Co.
29. Morini L, Piccolroaz A, Mishuris G. 2013 Dynamic energy release rate in couple-stress elasticity. *J. Phys.* **451**, 012014. (doi:10.1115/1.3629639)
30. Kaplunov J, Nobili A. 2017 A robust approach for analysing dispersion of elastic waves in an orthotropic cylindrical shell. *J. Sound Vib.* **401**, 23–35. (doi:10.1016/j.jsv.2017.04.028)